JGR Oceans

RESEARCH ARTICLE
10.1029/2025JC022509

Time Series of the Canary Current Derived From One Year of Pressure Inverted Echo Sounder (PIES) Data

A. Hernández-Guerra[1], **V. Caínzos**[1,2], **and P. Vélez-Belchí**[3]

[1]Unidad océano y clima, Instituto de Oceanografía y Cambio Global, IOCAG, Universidad de Las Palmas de Gran Canaria, ULPGC, Unidad Asociada ULPGC-CSIC, Las Palmas de Gran Canaria, Spain, [2]School of Earth and Atmospheric Sciences, Georgia Institute of Technology, Atlanta, GA, USA, [3]Centro Oceanográfico de Canarias, Instituto Español de Oceanografía, Santa Cruz de Tenerife, Spain

Abstract Five pressure inverted echo sounders (PIES) have been deployed north of the Canary Islands at a nominal latitude of 29°N for 1 year to estimate a time series of volume transport of the Canary Current (CC) and the Lanzarote passage (LP) using the gravest empirical method (GEM). The GEM method even detected a Mediterranean eddy flowing through one of the PIES. The absolute geostrophic velocity at the eastern islands is predominantly southward, while at the western islands, the velocity fluctuates between southward and northward. The highest absolute geostrophic velocity occurs in the LP, gradually decreasing significantly offshore. Both the CC and the LP exhibit strong variability, with mean southward volume transport of -1.4 ± 1.6 Sv and -0.4 ± 1.1 Sv, respectively. The CC shows a consistent southward volume transport across all seasons, with stronger flow in summer (-2.5 ± 1.4 Sv) and autumn (-2.1 ± 1.0 Sv), when the CC flows across the entire archipelago. The CC is weaker in spring (-0.3 ± 1.4 Sv) and winter (-0.8 ± 1.1) flowing through the eastern Canary Islands with a northward recirculation along the western islands. The LP exhibits a southward volume transport in spring (-1.1 ± 0.8 Sv) and winter (-0.9 ± 1.0 Sv), with a northward recirculation of the CC in summer (0.2 ± 1.0 Sv) and autumn (0.1 ± 1.0 Sv). Volume transport estimates from historical hydrographic cruises generally agree with those obtained from the PIES data. A cross-correlation of 0.71 shows that the seasonal cycle in the LP corresponds well with the seasonal cycle of the Atlantic meridional overturning circulation.

Plain Language Summary The Canary Current flows along the African coast and through the Canary Islands, forming the eastern boundary of the North Atlantic subtropical gyre. It connects with the Gulf Stream to the west, the Azores Current to the north, and the North Equatorial Current to the south This study presents the first-ever time series of the Canary Current. Furthermore, we have identified a strong correlation between the seasonal cycle of the Canary Current through the western islands and the seasonal cycle of the Atlantic meridional overturning circulation.

Key Points:

- Volume transport estimates derived from PIES data generally agree with those from historical hydrographic cruises
- The Canary Current is quite weak, with stronger velocities in the eastern basin
- The seasonal cycle of volume transport through the eastern islands closely matches the seasonal cycle of the AMOC

Supporting Information:

Supporting Information may be found in the online version of this article.

Correspondence to:

A. Hernández-Guerra,
alonso.hernandez@ulpgc.es

Citation:

Hernández-Guerra, A., Caínzos, V., & Vélez-Belchí, P. (2025). Time series of the Canary Current derived from one year of pressure inverted echo sounder (PIES) data. *Journal of Geophysical Research: Oceans*, *130*, e2025JC022509. https://doi.org/10.1029/2025JC022509

Received 15 FEB 2025
Accepted 21 JUL 2025

Author Contributions:

Conceptualization: A. Hernández-Guerra, V. Caínzos, P. Vélez-Belchí
Formal analysis: A. Hernández-Guerra
Investigation: P. Vélez-Belchí
Methodology: V. Caínzos, P. Vélez-Belchí
Software: V. Caínzos
Supervision: V. Caínzos
Validation: P. Vélez-Belchí
Writing – original draft: A. Hernández-Guerra
Writing – review & editing: V. Caínzos, P. Vélez-Belchí

1. Introduction

The Canary Current system (CCS) is a weaker current flowing southward within the thermocline, at an approximate depth range of 0–700 m. It flows along the eastern boundary of the North Atlantic subtropical gyre (NASG), which is formed by the Azores Current (AC) in the north and the North Equatorial Current (NEC) in the south (Stramma, 1984; Stramma & Isemer, 1988). The main water mass transported in the CCS is the North Atlantic central water (NACW) (Harvey & Arhan, 1988).

The AC flows to the east south of the Azores archipelago, with a net mass transport of approximately 8.5 Sv (1 Sv = 10^6 $m^3/s \approx 10^9$ kg/s; the positive/negative sign indicating a northward/southward or eastward/westward flow), accounting for its countercurrent (Comas-Rodríguez et al., 2011). It splots into several southward-moving branches (Käse & Siedler, 1982; Tychensky et al., 1998). The easternmost branch feeds the CCS, which flows parallel to the African coast and through the Canary Islands (Hernández-Guerra et al., 2005; Pérez-Hernández et al., 2013). Then, the CCS turns westward, feeding the NEC as the southern boundary of the NASG (Fiekas et al., 1992). Previous studies have divided the CCS into two main flows based on the different dynamics in each region: the primary flow through the islands, referred to as the Canary Current (CC), and the flow through the area between Lanzarote-Fuerteventura and the African shelf, known as the Lanzarote passage (LP) (Hernández-Guerra et al., 2017; Machín et al., 2010; Vélez-Belchí et al., 2021).

Machín et al. (2006), through a series of four hydrographic cruises conducted in each season during 1997–1998, found a southward mean mass transport of -2.1 ± 0.9 Sv through the Canary Islands and -0.6 ± 0.1 Sv across the LP. They also observed a seasonal shift in the path of the CC, with the current migrating from the eastern islands to the western islands between autumn and spring. This circulation pattern also varies interannually. For instance, Pérez-Hernández et al. (2023) processed four surveys carried out in 2015, one per season, and observed the CC in its easternmost position during winter and its westernmost position during autumn, with the current flowing through the entire Canary Islands in spring and summer. Across the LP, these studies have consistently reported a southward flow in every season except in autumn, where a northward recirculation, ranging from 0.8 to 1.9 Sv, has been observed as previously measured with XBT data and current meters moored in the LP (Fraile-Nuez et al., 2010; Hernández-Guerra et al., 2002, 2003). This pattern of a weak CC flowing to the south through the Canary Islands and the LP, except in autumn, has been repeatedly confirmed with in situ data and models (Casanova-Masjoan et al., 2020; Hernández-Guerra et al., 2017; Laiz et al., 2012; Mason et al., 2011).

As a result of the blockage caused by the Canary Islands on the CC and the persistent southward trade winds, cyclonic and anticyclonic eddies are generated downstream of the islands (Hernández-Guerra et al., 1993; Pacheco & Hernandez-Guerra, 1999; Sangrà et al., 2009). In addition, upwelling filaments, characterized by lower temperature and higher chlorophyll concentration, extend from the northwest African upwelling system to waters south of the Canary Islands (Barton et al., 1998; Borges et al., 2004; Van Camp et al., 1991). The mesoscale eddies generated south of the islands are present year-round. However, the occurrence of upwelled waters in the northwest African upwelling system and, therefore, the upwelling stretching to south of the islands, presents a seasonal behavior linked to the meridional displacement of the Azores High (Mittelstaedt, 1983). The most favorable season for upwelling in area of the Canary Islands is summer in which the Azores High is in its northernmost location (Hernandez-Guerra & Nykjaer, 1997; Marcello et al., 2011; Nykjær & Van Camp, 1994). Therefore, we decided to deploy our instruments north of the islands to avoid the influence of these patterns, which are responsible for the seasonal high kinetic energy detected south of the Canary archipelago (Barceló-Llull et al., 2017; Sangrà et al., 2009).

The seasonal cycle of the Atlantic meridional overturning circulation (AMOC) is connected to the density seasonal cycle at thermocline and intermediate layers along the eastern boundary (Chidichimo et al., 2010; Kanzow et al., 2010). During spring and autumn, the AMOC experiences maximum positive and negative density anomalies, respectively, leading to a decrease of the AMOC in spring and an increase in autumn, with an amplitude of 5.2 Sv, dominating the 6.7 Sv peak-to-peak seasonal cycle of the total AMOC. Pérez-Hernández et al. (2015, 2023) and Vélez-Belchí et al. (2017) found that this seasonal behavior of the AMOC is linked with the seasonal flow at the LP at the thermocline and intermediate layers. The increase of the AMOC in autumn is attributed to the northward recirculation of the CC across the LP (Hernández-Guerra et al., 2017). They concluded that the seasonal cycle of the AMOC is primarily driven by the dynamics of the eastern boundary current system, specifically, to the circulation and recirculation patterns along the LP.

Most of these studies, with the exception of 9 years of current meter data in the LP, have been conducted using hydrographic stations at specific months and years. In November 2022, five pressure inverted echo sounders (PIES) were deployed north of the Canary Islands to obtain a continuous time series of volume transport for the entire CC. PIES are bottom-mounted instruments that provide continuous measurements of bottom pressure and acoustic travel time (τ) to the sea surface, enabling the reconstruction of dynamic height profiles and geostrophic velocity estimates when combined with historical hydrographic data. PIES typically emit narrow band acoustic pulses at 12 kHz, balancing the signal range and resolution. To isolate the surface return, the instruments use short-duration pulses and apply time windowing to filter out spurious reflections, including those from sidelobes or internal layers. Echo detection algorithms identify the first arrival corresponding to the sea surface. These features allow PIES to operate autonomously for extended periods, making them well suited for observing large-scale variability in boundary current systems. This study provides the first year of new data from PIES downloaded via telemetry at the eastern boundary of the NASG, as outlined in Section 2. Section 3 details the gravest empirical mode (GEM) method used to estimate temperature and salinity time series from round-trip acoustic travel times. Sections 4 and 5 describe the geostrophic velocity and the absolute volume transport of the CC and the LP. The results are discussed, and conclusion are provided in Section 6, along with suggestions for future research.

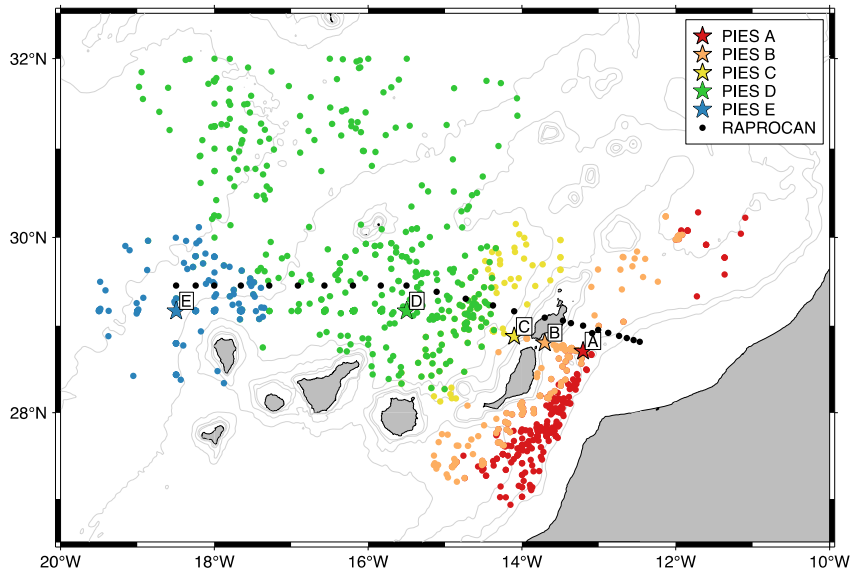

Figure 1. PIES locations in the Canary Islands. Every PIES is labeled with a letter and a corresponding color. The color of the dots represents hydrographic profiles used for the GEM calculations associated for each PIES. For improved clarity, the positions of the RAPROCAN CTD stations have been shifted 0.5° northward.

2. Data

In November 2022, five PIES were deployed north of the Canary Islands (Figure 1). Data were collected via acoustic telemetry during RAPROCAN hydrographic cruises in April and December 2023. Hydrographic stations at the location of the PIES were conducted to calibrate the PIES instruments. PIES measures the round-trip acoustic travel time (τ) and bottom pressure. Since τ is a function of the sound velocity, which depends on temperature and salinity throughout the water column, we can estimate these thermodynamics properties of the water column using the GEM procedure. Once these temperature and salinity fields are estimated, we can calculate the baroclinic component of geostrophic velocity. The barotropic contribution will be derived from the bottom pressure gradient and an estimation of the velocity at the reference layer. PIES data have been successfully applied in various oceanographic regions to determinate the local circulation (Book et al., 2002; Donohue et al., 2010; Meinen & Luther, 2003; Meinen & Watts, 2000; Meinen, Johns, et al., 2013; Meinen, Speich, et al., 2013; Meinen et al., 2018; Park et al., 2005; Rodrigues et al., 2010; Sun & Watts, 2001).

The specifications of the PIES deployed are detailed in Table 1. PIES A and B are positioned on the LP at depths of approximately 803 and 904 dbars, respectively. PIES C through E are strategically deployed to capture the flow of the CC through the Canary Islands. PIES C reaches a depth of about 2,133 dbar and is located only about 20 km away from Lanzarote Island due to the short continental shelf, a characteristic of the volcanic origin of the Canary Islands. PIES D is located north of Gran Canaria Island at the Canary Islands Ocean Time Series Station (ESTOC) at an approximate depth of 3,695 dbar. The westernmost instrument, PIES E, is positioned west of the western Canary Islands at a depth of about 4,309 dbar.

Table 1
Position and Depths of the PIES Deployed North of the Canary Islands

PIES	Latitude	Longitude	Depth (dbar)	CTD (<1,900)	CTD (>1,900)
A	28°40.7′	−13°05.2′	~803	331	—
B	28°48.1′	−13°42.3′	~904	231	—
C	28°52.5′	−14°06.1′	~2,133	90	80
D	29°09.9′	−15°30.1′	~3,695	304	237
E	29°10.0′	−18°29.2′	~4,309	48	143

Note. PIES A and B are situated in the Lanzarote passage (LP) while PIES C through E are located north of the Canary. The CTD column indicates the number of CTD casts shallower and deeper than 1,900 dbar used in the GEM method.

Figure 2 displays the measured and filtered τ and the measured, detrended, and filtered bottom pressure from PIES D (similar plots for the other PIES are shown in Figures S1 in Supporting Information S1). As shown in Figure 2a, τ oscillates between 4.816 and 4.818 s, except in April 2023, when it decreases to 4.812 s. This minimum τ is caused by a Meddy passing over PIES D. A Meddy is a mesoscale feature characterized by high temperature and salinity, which results in a higher sound velocity and, therefore, lower τ. Bottom pressure may show exponential and/or linear drifts that must be removed before applying filters (Donohue et al., 2010). For PIES D, the data reveal a single linear trend across the entire record. Figures 2a and 2c present both the

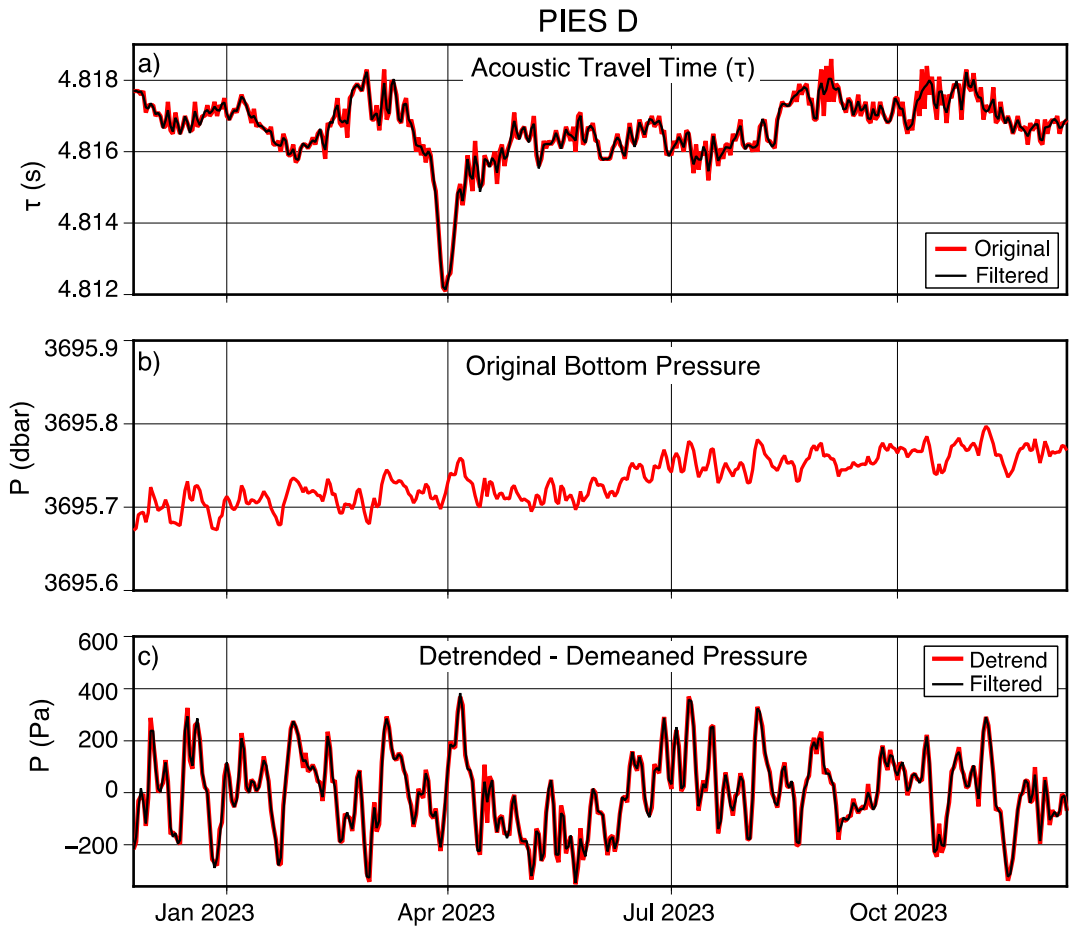

Figure 2. (a) Original and filtered (Butterworth filter with a 72-hr cutoff period) acoustic travel time (τ, in s), (b) original bottom pressure (P, in dbar), and (c) detrended and 3-day cutoff filtered bottom pressure (P, in pascal) for PIES D from 23 November 2022 to 8 December 2023. Figures S1 in Supporting Information S1 presents similar plots for PIES A, B, C, and E.

original and filtered data, processed using a Butterworth filter with a 72-hr cutoff period. The filtered records were then subsampled at 24-hr intervals.

The historical CTD data used in the gravest empirical method (GEM) to estimate temperature and salinity profiles from PIES data are obtained from two main sources: hydrographic sections surveyed routinely around the Canary Islands since 1996 and float data from the Argo program (Table 1). Only CTD profiles with appropriate potential temperature (θ)—salinity characteristics were selected from Argo data. Each PIES is associated with a large number of CTD profiles for GEM analysis. For each month, several CTD profiles are available for each PIES, so that the seasonal cycle can be removed. The hydrographic sections reach depths close the ocean floor, while Argo profiles only extend to 1,900 m depth, as shown for PIES C, D, and E in Table 1.

The volume transport estimated by the PIES data is compared with the volume transport derived from the CTD stations sampled during cruises north of the Canary Islands, primarily through RAPROCAN cruises. These stations are shown in Figure 1, with their positions shifted 0.5° northward for a better visualization. Additionally, at the LP, 9 years of volume transport have been estimated using a mooring installed in the middle of the passage (Fraile-Nuez et al., 2010; Hernández-Guerra et al., 2003).

3. The Gravest Empirical Method

A gravest empirical method (GEM) method has been applied to the PIES data to estimate the relationship between τ and the vertical profiles of temperature and salinity using a two-dimensional lookup table (Meinen & Watts, 2000; Watts et al., 2001). The GEM method consists in the use of historical CTD profiles collected near the

PIES location to infer this relationship. For the GEM to function effectively, sufficient historical hydrographical casts must be available to cover the entire range of the PIES τ in order to encompass the variability recorded by each PIES deployed in the Canary Islands area.

As seen in Figure 1, the hydrographic profiles used for PIES A, B, and C form a rectangle region, while those for PIES E are distributed within a circle with a radius of 100 km. In contrast, the CTD profiles associated with PIES D are more widely scattered because a Mediterranean eddy (Meddy) crossed the area of this PIES. Consequently, all CTD profiles showing evidence of the Meddy were included to ensure that the lookup table captured the full range of τ values observed by PIES D.

Table 1 summarizes the number of CTD profiles shallower than 1,900 dbar, derived primarily from Argo float data, and those deeper than 1,900 dbar for PIES C, D, and E. The number of CTD profiles for each PIES is substantial.

The GEM has been applied in various oceanographic areas where a smooth curved relationship between temperature/salinity and τ is observed, indicating the presence of distinct water mass at each specific depth (Meinen, 2001; Meinen, Johns, et al., 2013; Meinen, Speich, et al., 2013; Watts et al., 2001).

For the GEM, the CTDs corresponding to each PIES are used to adjust temperature and salinity at each pressure level (every 10 dbar) to a curve as a function of the simulated τ (Figure 3 for PIES D; similar plots for the remaining PIES are shown in Figures S2 of Supporting Information S1). Following the approach described by Meinen and Watts (2000), this adjustment is performed using a cubic smoothing spline from the surface to the bottom of the ocean. The values from the spline are extracted to a regular grid of τ with a resolution of 0.5 ms (1 ms = 10^{-3} s), matching the resolution of the PIES, across the entire range of the simulated τ (Figure 3). This process results in smooth grids of temperature and salinity as function of pressure and τ.

An exceptional case occurs in PIES D, where large τ values are observed due to the Meddy measured in April 2023. This may introduce a bias by attempting to fit an event that occupies only a small portion of the time series using a single cubic smoothing spline. To reduce this bias, one approach is to use two cubic smoothing splines: one for the low-τ region, associated with high Mediterranean water (MW) content due to Meddies and another for the remaining τ values. In any case, this method must be carefully implemented to avoid discontinuities between the two splines in the overlapping τ range.

The root mean square (RMS) error at each pressure level, indicated in the title of each subplot, is generally low, except near the surface (Figures 3a and 3i). This suggests that the GEM fields effectively capture a significant portion of the variance across all depths. Consequently, the GEM method is expected to provide reasonably accurate estimates of temperature (T) and salinity (S) when applied to PIES data.

The surface layer (<150 dbar) undergoes seasonal warming and cooling, causing τ to exhibit seasonal variability. To account for this, the CTD profiles associated with each PIES are distributed across the year, and the seasonal cycle is removed following the methodology of Tracey and Watts (1986). Using the CTD profiles collected throughout the year, the monthly mean temperature at different depths is calculated. The depth at which temperature does not exhibit a seasonal cycle—150 m in our case—is selected to determine τ for each month. The relative differences between the minimum τ and the τ values for the other months are then subtracted from each monthly value to remove the average seasonal cycle.

The resulting seasonally corrected GEM is calibrated using simulated τ from CTDs collected during the deployment period of the PIES. These CTDs were gathered in November 2022 and April and December 2023 coinciding with telemetry sessions for data retrieval. The τ time series are subsequently converted into τ time series at 700 and 800 dbar for PIES A and B, respectively, and at 1,900 dbar from PIES C to E. This conversion is based on the smooth curved relationship between τ integrated from the surface to the ocean bottom and τ integrated from the surface to these specific depths, as described by Meinen and Watts (1998). Thus, the lookup tables for temperature and salinity will be indexed by τ integrated from the surface to 800, 900, and 1,900 dbar for PIES A, B, and C–E, respectively. These depths are chosen because they lie below the thermocline layer, where ocean currents in the regions are most prominent, and they include a substantial number of float profiles from the Argo program.

The GEM field for temperature and salinity corresponding to PIES D is shown in Figures 4a and 4b, along with the root mean square error (RMSE) between the CTD measurements and the estimated profiles (Figures 4c and

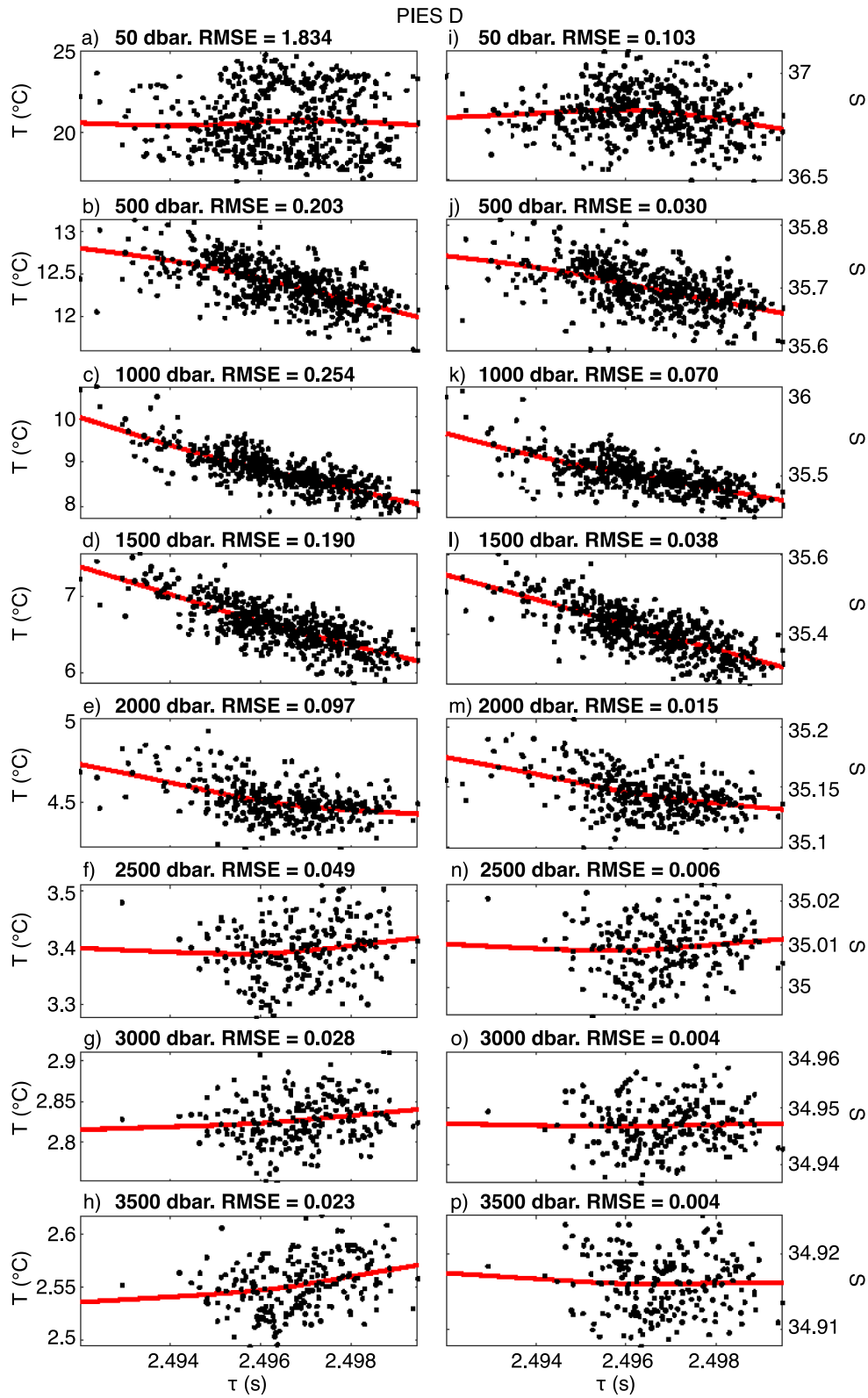

Figure 3. (a)–(h): Scatterplots of temperature (T, °C) versus acoustic travel time (τ, s) integrated from the surface to 1,900 dbar at several pressure levels every 500 dbar for PIES D. Each dot represents data from hydrographic profiles at locations shown in Figure 1. At each level, a cubic smoothing spline (red curve) is fitted to the data from the surface to the bottom every 10 dbars to generate a lookup table. (i)–(p) Scatterplots similar to (a)–(h) but for salinity. Root mean squared (RMS) differences are indicated in each subplot. Figures S2 in Supporting Information S1 presents similar plots for PIES A, B, C, and E.

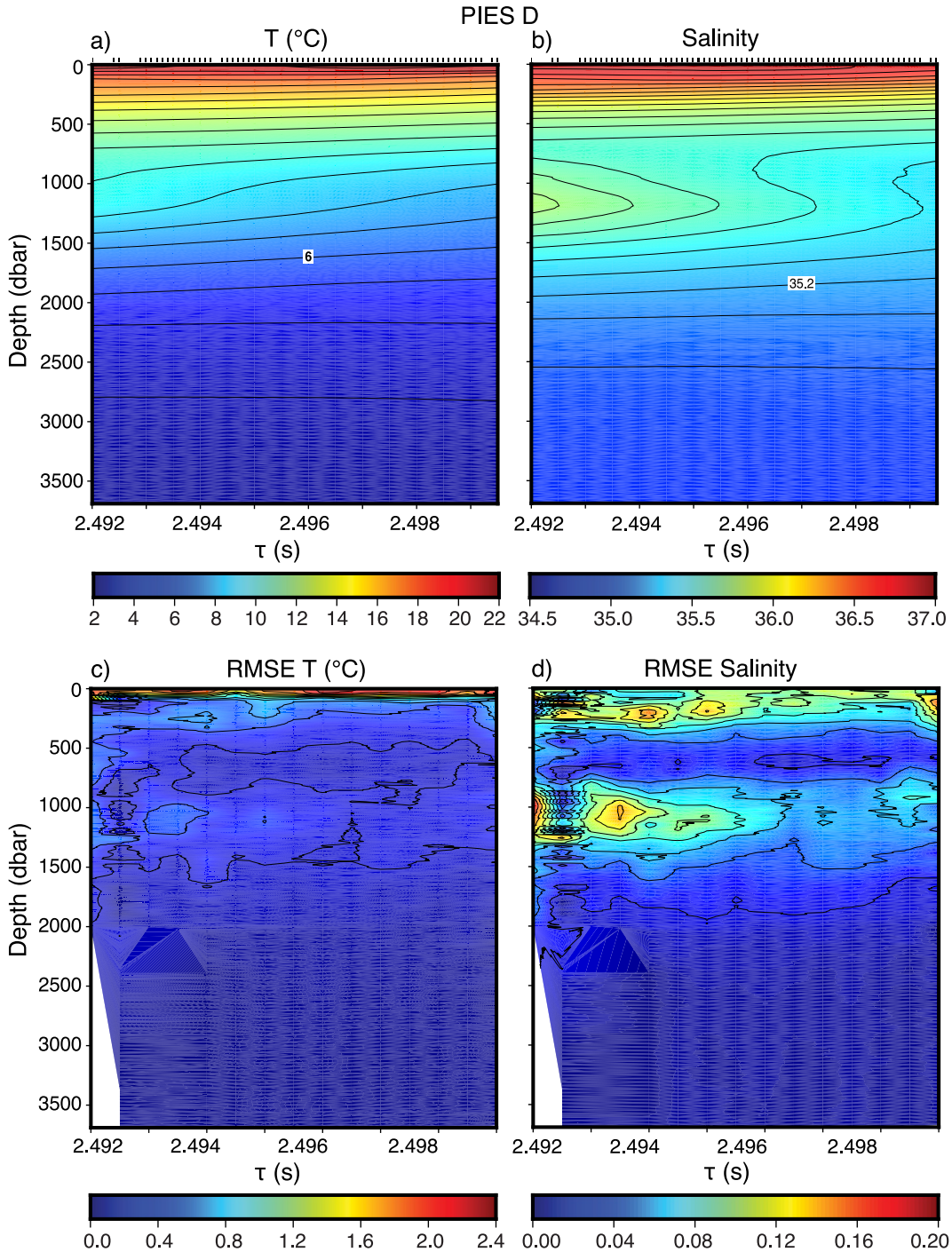

Figure 4. (a) Two-dimensional lookup table of temperature for various simulated travel times (τ) between the surface and the depth of PIES D using the GEM method, (b) same as (a) for salinity, and (c) and (d) root mean squared (RMS) differences for temperature and salinity, respectively, computed by comparing in situ CTD or Argo data with the corresponding GEM estimations. Figures S3 in Supporting Information S1 presents similar plots for PIES A, B, C, and E.

4d). Similar plots for the other PIES are provided in Figures S3 in Supporting Information S1. The GEM technique offers the full-water-column estimates of temperature and salinity for each τ. Higher or lower values of τ correspond to colder/fresher or warmer/saltier waters, respectively. Consequently, the intermediate layers at the right and left sides of Figures 4a and 4b represent Antarctic intermediate waters (AAIW) and Mediterranean waters (MW), respectively, indicating that the GEM captures water mass variability in the Canary Islands region.

Table 2
Standard Error (Sv) of the GEM Method Based on a Monte Carlo Approach Using the Estimated RMSE

	Standard error (Sv)		
	LP	Pies C-D	Pies D-E
Time-mean	0,31	0,51	0,56
Spring	0.16	0,26	0,27
Summer	0.15	0,25	0,28
Autumn	0,14	0,23	0,25
Winter	0,15	0,26	0,28

While the temperature and salinity profiles estimated by the GEM method are not as precise as actual CTD measurements, they successfully incorporate the major water masses.

Figures 4c and 4d illustrate the accuracy of the temperature and salinity profiles through the dispersion between the original observations and the values from the lookup table for PIES D. It is important to note that this difference does not represent the standard error of the mean but rather the oceanic variability around the mean temperature and salinity. The GEM method estimates the temperature (salinity) with a higher RSME of 1.83°C (0.10) at the surface (50 dbar) and 0.25°C (0.07) at the intermediate layers (1,000 dbar). The RSME decrease in the thermocline, reaching 0.20°C (0.03) at 500 dbar, and in the deep layers, dropping to <0.10°C (0.02) at depths greater than 2,000 dbar.

The high RSME values at the surface and intermediate layers are also observed across all the PIES. Near-surface high RSME values for both temperature and salinity are attributed to seasonal variability, which the GEM method does not account for. At intermediate layers, elevated RSME values arise from the variability of temperature and salinity within the AAIW and MW water masses, which coexistent in these depths. Additionally, for very short τ, no CTD data are available at depths below 1,900 dbar, as this corresponds to the limit of Argo data availability.

To estimate the error of the GEM method, we have applied the Monte Carlo approach, following a methodology previously used by Hernández-Guerra et al. (2002) to quantify the uncertainty in mass transport estimates derived from XBT data. For each pressure level, we generated 1,000 random pairs of temperature and salinity values (Ti and Si), assuming both variables follow normal distributions centered on their mean values at that pressure level ($\overline{T}$ and $\overline{S}$). The variability around these means was defined using the root mean square error ($RMSE_T$ and $RMSE_S$, respectively), so that

- $Ti \sim N(\overline{T}, RMSE_T)$
- $Si \sim N(\overline{S}, RMSE_S)$

Each pair (Ti and Si) was then used to compute a corresponding value of volume transport. The resulting distribution of 1,000 volume transport estimates allowed us to assess the standard error as shown in Table 2.

4. Geostrophic Velocity

Figure 5 displays the results of τ data from PIES D, converted into GEM-derived mean profiles of temperature and salinity, alongside the corresponding time series of temperature and salinity anomalies. The time series clearly highlights the presence of a Meddy around April 2023, characterized by higher temperature and salinity anomalies at intermediate layers than the rest of the series. Anomalies of temperature and salinity at depths greater than 2,000 dbar are minimal, consistent with observations from PIES C and E, as shown in Figures S4 in Supporting Information S1. Consequently, the velocity shear between PIES C and D, as well as between PIES D and E, is expected to remain approximately zero from about 2,000 dbar to the bottom of the ocean.

The baroclinic and the barotropic anomaly contributions of the total geostrophic velocity are estimated using PIES data (Meinen, Johns, et al., 2013; Meinen, Speich, et al., 2013). The time series of baroclinic component is derived from specific volume anomaly profiles, calculated using the time series of temperature and salinity estimated by the GEM, as shown in Figure 5. The geopotential height anomaly ($\Delta\Phi$) is then obtained by vertically integrating the specific volume anomaly profiles vertically.

From each PIES pair, the $\Delta\Phi$ profiles are subtracted to find the component of the relative velocity perpendicular to the line connecting the PIES, using the standard dynamic method. The resulting velocity time series are referenced to an assumed level of no motion, set at 870 dbar for PIES pair A-B and 1,900 in PIES pairs C-D and D-E.

The variability of the barotropic component is estimated from the pressure gradient in each PIES pair from the geostrophic equation (Meinen & Watts, 2000). This approach provides the fluctuations in barotropic geostrophic

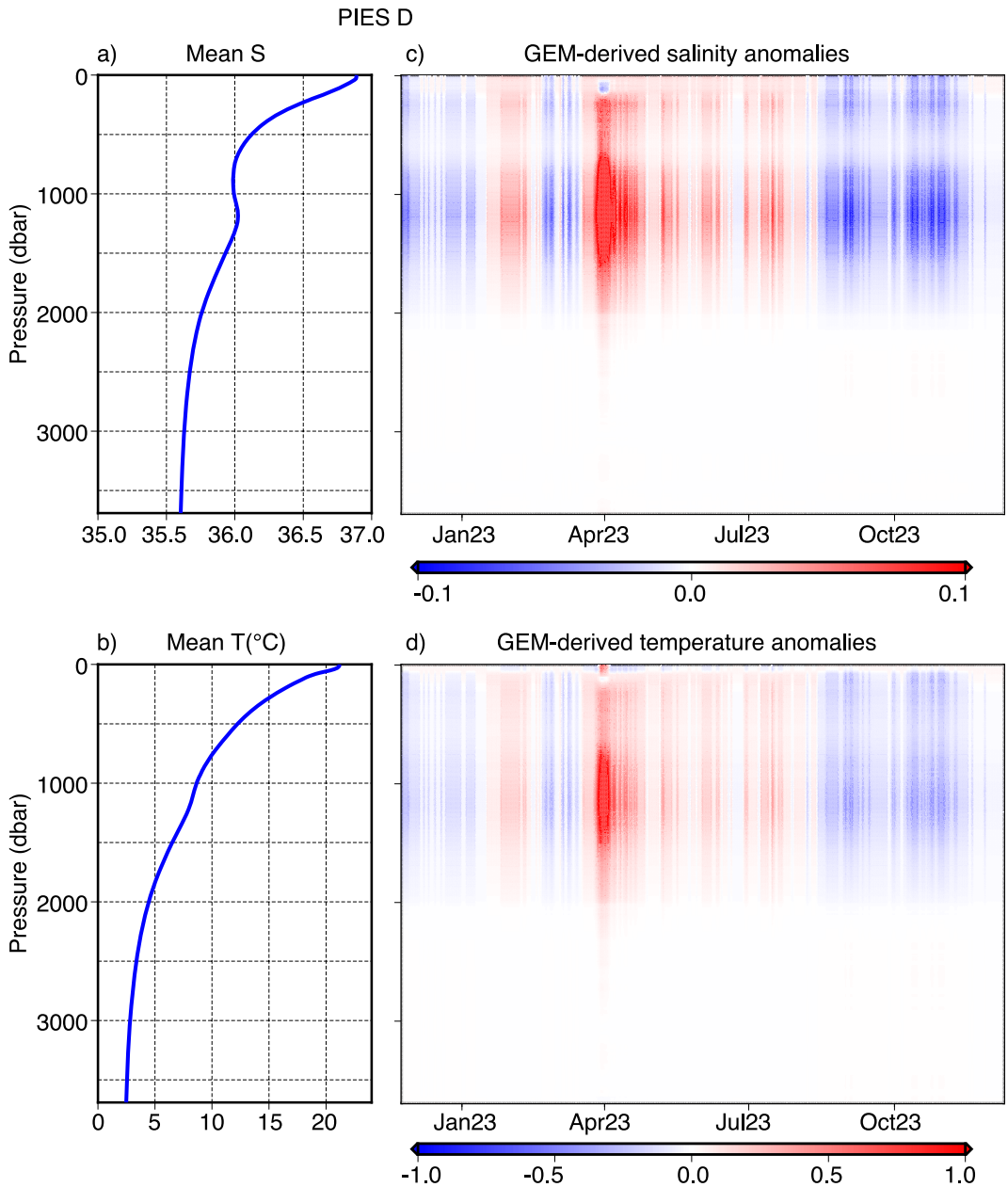

Figure 5. (a) Vertical profile of mean potential temperature for PIES D, (b) time series of potential temperature anomalies for PIES D, derived using the GEM lookup table applied to the 3-day cutoff filtered acoustic travel time (τ) for PIES D, and (b) and (c): same as (a) and (b) but for salinity. Figures S4 in Supporting Information S1 presents similar plots for PIES A, B, C, and E.

velocity but not the time-mean velocity due to the well-known leveling problem, which arises from the uncertainty in the vertical positioning of each PIES relative to a constant geopotential surface (Donohue et al., 2010).

In this study, the time-mean velocity is estimated using in situ and model results, following the method outlined by Meinen et al. (2012). For PIES pair A-B, the time-mean velocity is derived from the 9 years of current meter data at the LP, yielding a value of 0.9 cm/s at 870 m (Fraile-Nuez et al., 2010; Hernández-Guerra et al., 2003). For PIES pair C-D and D-E, the time-mean velocity is obtained from the average velocity at 1,900 m depth based on 29 years of GLORYS numerical modeling result. At this depth, PIES C-D and D-E have lower velocities of 7.9×10^{-2} cm/s and 3.9×10^{-2} cm/s, respectively.

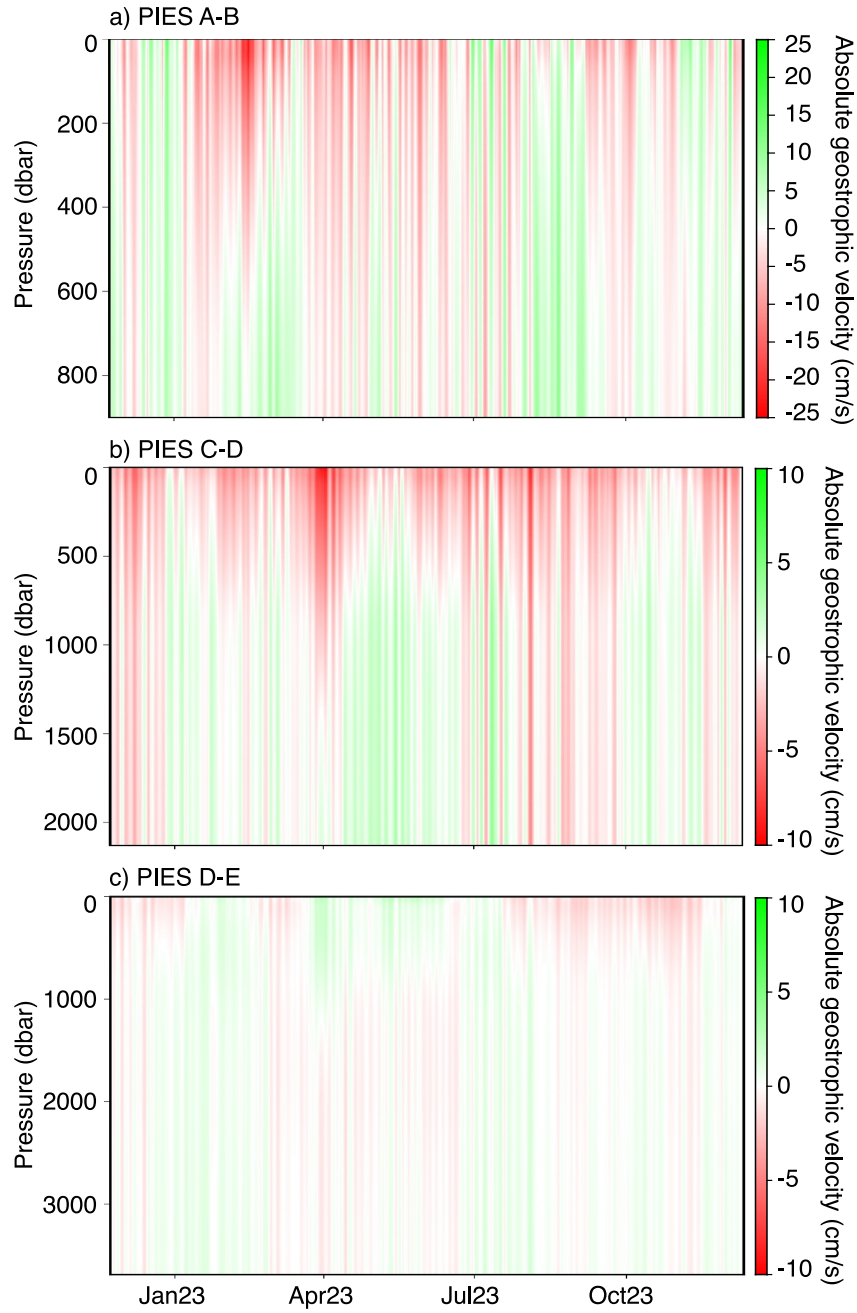

Figure 6. Absolute geostrophic velocity (cm/s) perpendicular to the section connecting the following PIES pairs: (a) A-B, (b) C-D, and (c) E-D. It should be noted that the scale in panel (a) exceeds that of panels (b) and (c) by more than a factor of two.

As a result, the full-water-column time series of absolute velocity perpendicular to the line connecting PIES pair A-B, C-D, and D-E is estimated (Figure 6). The highest absolute geostrophic velocity in PIES pair AB (∼−24 cm/ to the south) is more than double that of the highest velocity in PIES pair C-D (∼−10 cm/s), which, in turn, is higher than the maximum velocity in PIES pair D-E (∼−3 cm/s).

The LP (PIES A-B), as shown in Figure 6a, exhibits a predominantly southward flow from January to November, with a brief period of northward flow during the first/second fortnight of July/August. Recirculation of the flow in the LP is observed in December 2022 and November 2023. The LP shows a smaller average southward absolute

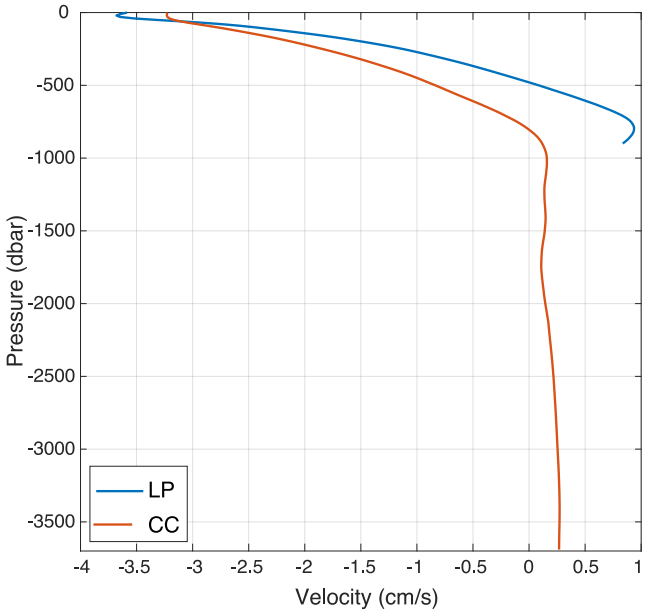

Figure 7. Vertical profile of the time-mean absolute geostrophic velocity (cm/s) for the Canary Current (CC, PIES C-E) and the Lanzarote passage (LP, PIES A-B). The transition depth between southward (negative) and northward (positive) velocities occurs at approximately 480 dbar in the LP and 810 dbar in the CC.

geostrophic velocity of −3.5 cm/s at 10 dbar, although it spans a considerable range, with a maximum southward velocity of −24.2 cm/s and maximum northward velocity of 15.4 cm/s velocity at the same depth.

The CC (PIES C-E) exhibits considerably lower velocities than the LP (Figures 6a and 6b). The mean velocity at 10 dbar for PIES pair C-D is −3.1 cm/s, while for PIES pair D-E is −0.1 cm/s. The influence of the Meddy passing through PIES D is evident in the high southward and northward velocities observed in April in PIES pair C-D and D-E up to ∼1,000 dbar, respectively. Velocity at the PIES pair C-D is predominantly southward, whereas the velocity at PIES pair D-E shows greater variability, alternating between southward and northward flows.

At 10 dbar, the maximum southward velocity for PIES pair C-D is −9.8 cm/s, attributed to the Meddy. Despite the Meddy crossing the area around PIES D, this maximum velocity remains lower than that in the LP. The maximum southward velocity for PIES pair D-E is −2.5 cm/s. The maximum northward velocity for pair PIES C-D and D-E are 1.2 and 2.8 cm/s, respectively. This northward maximum velocity for the PIES pair D-E is also attributed to the Meddy.

Figure 7 shows the estimated time-mean velocity for the LP and the offshore CC. Both profiles align with the expected patterns: a weak southward flow in the shallower layers (<4 cm/s); a northward transport in intermediate layers in the LP; and a weaker, almost barotropic northward flow the in deeper layers of the CC. The transition depth between southward (negative) and northward (positive) velocities occurs at approximately 480 dbar in the LP and 810 dbar in the CC.

Previous studies carried out in the Canary Islands have chosen $\gamma^n = 27.38$ kg/m^3 as the boundary separating NACW from Antarctic Intermediate Water (AAIW) defining the thermocline layer. This layer is located at about 740 dbar (see, e.g., Pérez-Hernández et al. (2023)), closely coinciding with the transition depth of northward/southward velocity in the CC. However, in the LP, the $\gamma^n = 27.38$ kg/m^3 layer is deeper than the observed transition depth.

If we only consider the southward component of the LP velocity time series, excluding the recirculation of the CC in the LP, the transition depth increases to 690 dbar, closely aligning with the boundary of the thermocline layer. It is important to note that $\gamma^n = 27.38$ kg/m^3 was selected as the reference layer for integrating the thermal wind equation with an initial null velocity, but it does not necessarily represent the final transition reference depth after applying an inverse model that corrects the velocity at the reference level for achieving mass balance.

The transition depth estimated in the Canary Islands area is shallower than those estimated at 26.5°N (∼1,100–1,160; Cunningham et al. (2007)) and at 34.5°S (∼1,170 dbar; Meinen, Johns, et al. (2013) and Meinen, Speich, et al. (2013)).

5. Absolute Volume Transport

PIES data have proven to be valuable for estimating volume transport (Meinen, Johns, et al., 2013; Meinen, Speich, et al., 2013; Meinen & Watts, 2000). Absolute volume transport is calculated based on the absolute geostrophic velocity, and the area comprised by the distance between the PIES and the vertical sampling interval (10 dbar). As a result, it is directly proportional to the absolute geostrophic velocity. Additionally, time series of Ekman transport, derived from ERA5 winds, are incorporated to the shallowest layer.

The integration of absolute volume transport from the surface down to 810 dbar for the CC and 690 dbar for the LP provides the respective time series of the CC and the flow through the LP. Both the original volume transport data and the 10-day Butterworth-filtered series are presented in Figure 8. Volume transport referred to below corresponds to the filtered time series data.

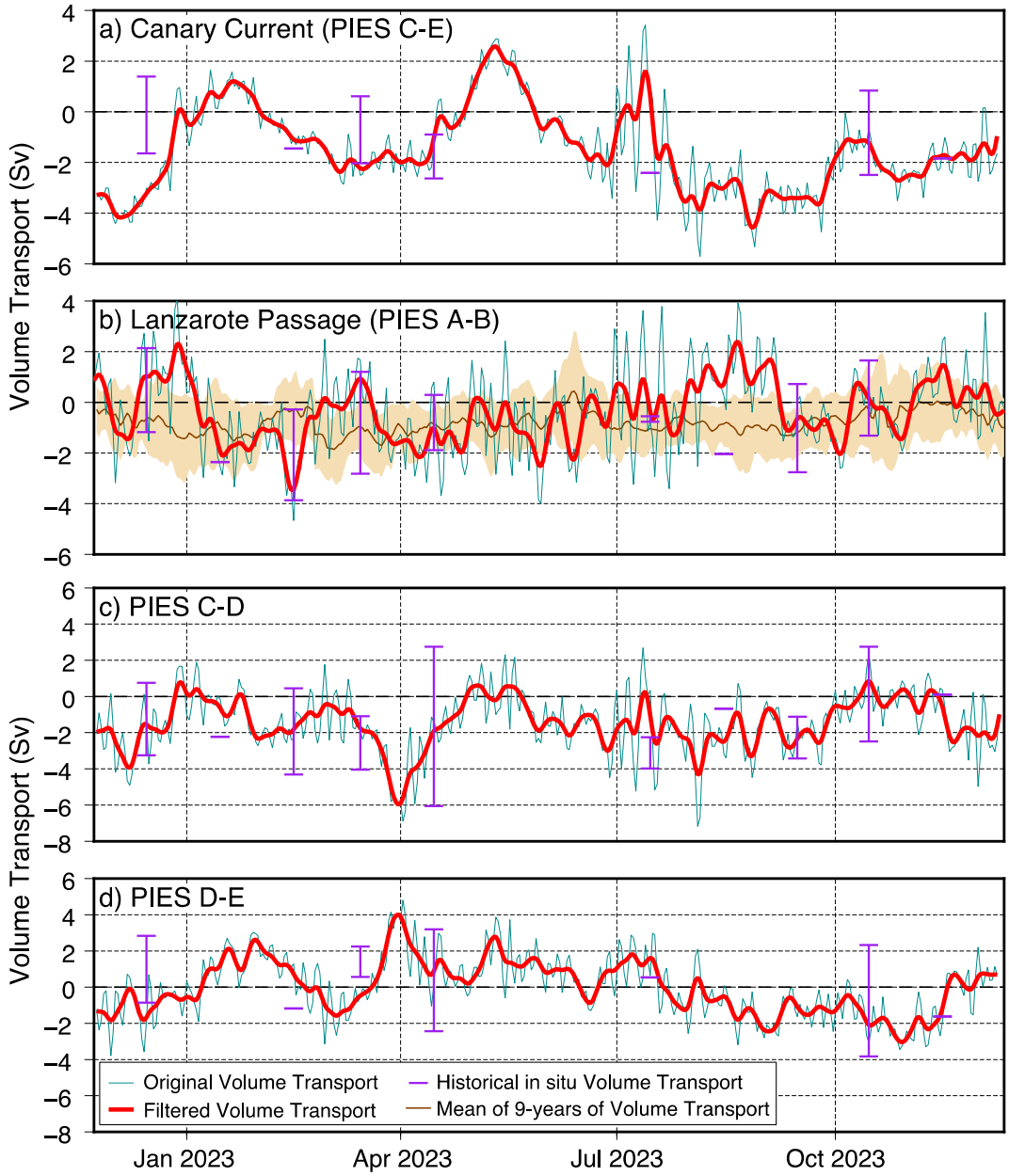

Figure 8. Original and 10-day filtered volume transport time series for (a) the Canary Current (CC), (b) the Lanzarote passage (LP), (c) the section between PIES C and D, and (d) the section between PIES D and E. In situ mean volume transport measurements, along with their standard deviations, for various months from all RAPROCAN cruises are included in each subplot. Additionally, the 9-year volume transport mean for the Lanzarote passage (LP) is shown.

As shown in Figure 8a, the CC (PIES C-E) exhibits significant temporal variability, with a mean southward volume transport of −1.4 ± 1.6 Sv during the year of study (Table 3). The maximum southward transport occurs in August, reaching −4.6 Sv. On several occasions, the CC flows northward, with maximum transports of 2.6 Sv, occurring in May.

The mean transport of the CC is primarily concentrated in the eastern part of the region, between PIES C and D (Table 3 and Figures 8c and 8d). The mean transport in PIES C-D is −1.4 ± 1.3 Sv, while the mean transport in PIES D-E has zero mean (0.0 ± 1.4 Sv). The observed northward transport in the CC during certain months is attributed to northward circulation in PIES D-E. The presence of a Meddy is evident, with maximum southward and northward volume transport of −6.0 and 4.0 Sv observed in April 2023 in PIES C-D and D-E, respectively.

Table 3
Time-Mean and Seasonal Averages of the Volume Transport for the Canary Current (CC) and Lanzarote Passage (LP) Derived From PIES Data

	Volume transport (Sv)			
	CC	LP	Pies C-D	Pies D-E
Time-mean	−1.4 ± 1.6	−0.4 ± 1.1	−1.4 ± 1.3	0.0 ± 1.4
Spring	−0.3 ± 1.4	−1.1 ± 0.8	−1.4 ± 1.4	1.1 ± 0.8
Summer	−2.5 ± 1.4	0.2 ± 1.0	−1.9 ± 0.9	−0.6 ± 1.2
Autumn	−2.1 ± 1.0	0.1 ± 1.0	−1.0 ± 1.2	−1.1 ± 1.0
Winter	−0.8 ± 1.1	−0.9 ± 1.0	−1.5 ± 1.4	0.7 ± 1.4

In the LP, variability in volume transport is also observed (Table 3). The mean volume transport is also southward (−0.4 ± 1.1 Sv), with maximum southward and northward volume transport of −3.5 and 2.4 Sv in February and in August, respectively (Figure 8b). Northward volume transport exceeding 1 Sv in the LP is recorded during autumn 2022 and 2023, as well as summer 2023.

Figure 8 also includes the in situ volume transport from the RAPROCAN cruise in each subplot, as well as the 9-year mean volume transport for the LP (Figure 8b). The volume transport of each RAPROCAN cruise has been estimated using the thermal wind equation for each station pair (Figure 1) and then summing the results for all station pairs corresponding to each PIES pair. The same reference layer velocity and Ekman transport have been applied. To ensure consistency, the vertical integration of the volume transport has been chosen in the same way as for the PIES data.

In both the CC and the LP, the composite volume transports estimated by the RAPROCAN cruises generally overlap the time series of the volume transport from the PIES in each month, considering the high variability of the volume transport calculated from the RAPROCAN data (Figures 8a and 8b). This pattern is also observed in the volume transport for PIES segments C-D and D-E (Figures 8c and 8d). However, some differences arise when comparing these results to the 9-year mean of volume transport (Figure 8b).

The 9-year mean transport was derived from data collected by a mooring deployed in middle of the LP, with the shallowest current meter at a depth of 150 m depth (Fraile-Nuez et al., 2010; Hernández-Guerra et al., 2003). These mean transports were estimated by comparing the data from the central mooring with transport measurements obtained using four moorings equipped with a total of 19 current meters, which spanned the entire passage during the two first 2 years of study. For the thermocline layer, a regression coefficient of $R^2 = 0.57$ was obtained, which could explain the differences between the volume transport time series estimated from PIES and from the current meters.

Table 3 presents the seasonal volume transport for the CC and the LP based on the PIES data. The mean flow of the CC is to the south in every season. Significant southward volume transport is observed during summer (−2.5 ± 1.4 Sv) and in autumn (−2.1 ± 1.0 Sv). The volume transport across PIES C-D and D-E provides the pathway of the CC. In autumn, the CC flows across the entire Canary Islands (through PIES C-D and D-E), whereas in summer, it primarily flows through the eastern islands (PIES C-D). During spring and winter, the CC flows along the eastern islands (PIES C-D), with a northward transport occurring through the western islands (PIES D-E).

In the LP, the mean volume transport is to the north during summer (0.2 ± 1.0 Sv) and autumn (0.1 ± 1.0 Sv), whereas in spring (−1.1 ± 0.8 Sv) and winter (−0.9 ± 1.0 Sv), it is southward with higher mean values. As discussed previously, the northward flow results from the recirculation of the CC.

6. Seasonal Cycle of the Atlantic Meridional Overturning Circulation

The Atlantic meridional overturning circulation (AMOC) exhibits a seasonal behavior. Chidichimo et al. (2010) identified a seasonal cycle in density at the eastern boundary, with maximum negative anomalies in autumn, corresponding to peak AMOC transport, and minimum transport in spring. Kanzow et al. (2010) established that the eastern boundary plays a key role in controlling the seasonal variability of the AMOC.

These findings, based primarily on observational data from the RAPID program, have been further supported by modeling studies (Duchez et al., 2014; Mielke et al., 2013; Yang, 2015; Zhao & Johns, 2014). These studies have proposed distinct mechanisms to explain the AMOC's seasonal behavior, ranging from wind stress curl at the eastern boundary to a seasonal redistribution of water mass volume driven by both local and remote wind stress.

Another plausible mechanism for the seasonal behavior of the AMOC is the flow at the LP, as first described by Pérez-Hernández et al. (2015). Pérez-Hernández et al. (2023) and Vélez-Belchí et al. (2017), using results from inverse models applied to a combination of hydrographic data, the mooring installed in the LP, and altimetry data, indicated a seasonal cycle across the LP that aligns with the seasonal cycle of the AMOC. The range of both seasonal cycles are approximate similar (Casanova-Masjoan et al., 2020).

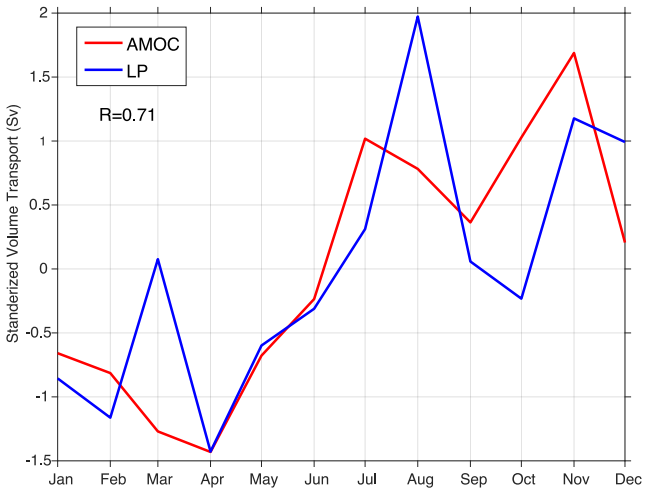

Figure 9. Seasonal cycle of standardized transport (Sv) of the Atlantic meridional overturning circulation (AMOC) obtained from the RAPID-MOCHA array, compared with the volume transport across the Lanzarote passage (LP) estimated using PIES A-B.

Figure 9 presents the seasonal cycle of the AMOC derived from the Rapid Data spanning from 2 April 2004 to 11 February 2023, alongside the seasonal cycle of the volume transport in the LP using the PIES data. Both time series have been standardized. Standardization is a common technique used to normalize time series data. The most widely used method involves subtracting the mean and dividing each data point by the standard deviation. This transformation centers the data around zero and scales it to have a standard deviation of one, making the data easier to analyze by placing it on a consistent scale.

The correlation between both standardized time series is strong, with a value of 0.71, despite having only 1 year of volume transport data available for the LP.

7. Discussion and Conclusions

There is no single standard for selecting CTDs to be used in the GEM method. In this study, CTDs were chosen around each PIES to minimize the likelihood of mixing different water masses that may overlap at the same depth. For example, AAIW has a stronger influence in the LP region, whereas MW is more dominant around the western islands. However, this approach could not be applied to PIES D due to the presence of a Meddy. In this case, all historical CTD profiles that had observed a Meddy near the Canary Islands were used for the GEM method applied to PIES D.

Volume transport for 1 year north of the Canary Islands has been estimated using PIES data. The PIES were strategically deployed north of the islands to avoid interference from cyclonic and anticyclonic eddies generated south of the islands (Pacheco & Hernandez-Guerra, 1999). These eddies, formed by the interaction of the CC and trade winds with the islands, carry substantial kinetic energy comparable to that of the CC itself (Sangrà et al., 2009).

It is important to acknowledge that the volume transport of the CC estimated from the PIES maybe influenced by cyclonic or anticyclonic eddies passing through the easternmost PIES E. In this context, Hernández-Guerra et al. (2005) identified a significant number of mesoscale eddies in a section carried out north of the Canary Islands, although these were smaller and less energetic than those formed south of the islands. These eddies can lead to an overestimation or underestimation of the CC transport in the D-E transect. A case in point is the Meddy observed passing through PIES D, which, along with the CC, resulted in a combined volume transport of −6.0 Sv southward across C-D and 4.0 Sv northward across D-E. This yields a net southward volume transport of −2.0 Sv, which aligns closely with the mean CC transport. If PIES D had been the final instrument, the estimated CC transport in April would have appeared strong.

Earlier studies in the Canary Islands region have estimated mass transport instead of volume transport. For the data obtained from the PIES, we opted to compute volume transport instead. This approach avoids the need to estimate density from the temperature and salinity profiles derived from the GEM method, which would introduce a degree of uncertainty into the mass transport calculations. Although this limits direct comparison with previous studies, the density of seawater is close to 1,000 g/m^3, making mass transport roughly equivalent to volume transport. Another factor to consider when comparing our results with those from previous studies is that the earlier studies conducted cruises lasting approximately 13 days per season. However, the mass transport derived from box inverse models in those studies was assumed to be representative of the entire season.

The volume transport derived from PIES data, from hydrographic data collected during RAPROCAN cruises north of the Canary Islands, and from currentmeter data installed in the LP show strong agreement in magnitude despite differences in timing and the locations of the shallowest currentmeter (Figure 8).

The CC transport ranges from −4.6 Sv southward to 2.6 Sv northward, with a mean southward transport of −1.4 ± 1.6 Sv. This is consistent with the −2.1 ± 0.9 Sv reported by Machín et al. (2006) from four hydrographic sections north of the islands in 1997–1998. Similarly, Pérez-Hernández et al. (2023) estimated a lower but comparable mean mass transport of −0.5 ± 1.4 Sv using data from four cruises in 2015.

In spring, the CC volume transport derived from PIES (−0.3 ± 1.4 Sv) is lower than previous estimates (−2.8 ± 0.8 Sv by Machín et al. (2006) and −2.1 ± 0.7 Sv by Pérez-Hernández et al. (2023)). This discrepancy is likely due to strong interannual variability, as noted by Casanova-Masjoan et al. (2020), who reported a transport of −0.7 ± 0.2 Sv in the spring of 2016 and −3.9 ± 0.4 Sv in the spring of 2017. In this season, the main path of the CC is through the eastern islands (−1.4 ± 1.4 Sv) with a northward flow (1.1 ± 0.8 Sv) across the western islands.

The strongest southward volume transport of the CC (−2.5 ± 1.4 Sv) occurs in summer, consistent with the previous estimations of −2.9 ± 0.8 Sv by Machín et al. (2006) and −2.0 ± 0.6 Sv by Pérez-Hernández et al. (2023). During this season, the main path of the CC is through the eastern islands (PIES C-D: −1.9 ± 0.9 Sv), although a significant volume is also transported through the western islands (PIES D-E: −0.6 ± 1.2 Sv), as reported in earlier studies.

In autumn, PIES data indicate southward CC transport (−2.1 ± 1.0 Sv), comparable to the −2.7 ± 0.4 Sv reported by Machín et al. (2006). However, Pérez-Hernández et al. (2023) observed a northward transport of 2.0 ± 0.6 Sv in 2015. This discrepancy maybe attributed to significant CC meandering and zonal shifts during autumn. For instance, Machín et al. (2006) observed the CC flowing across the eastern islands with a mass transport of −2.7 ± 0.4 Sv, while Pérez-Hernández et al. (2013) reported a mass transport of −6.2 ± 0.6 Sv west of the outer western islands. This high mass transport is likely due to the westward migration of the CC and its convergence with another branch of the Azores Current (Stramma & Siedler, 1988). The northward flow detected in autumn maybe also associated to a northward recirculation of the CC flowing west of the archipelago. Additionally, Hernández-Guerra et al. (2017) estimated a mass transport of −1.5 ± 0.7 Sv in 2014 across the entire Canary Islands. This observation is also reflected in our results, as the volume transport across the eastern islands (−1.0 ± 1.2 Sv through PIES C-D) is comparable to that across the western islands (−1.1 ± 1.0 Sv through PIES D-E).

In winter, the PIES data estimate a transport of −0.8 ± 1.1 Sv, which is similar to the −0.7 ± 0.6 Sv reported by Machín et al. (2006). Pérez-Hernández et al. (2023) estimated a northward volume transport of 0.2 ± 0.8 Sv, which is consistent with our time series because the volume transport from the PIES data is northward in January 2023. During this season, the CC flows across the eastern islands (−1.5 ± 1.4 Sv) with a northward recirculation through the western islands (0.7 ± 1.4 Sv).

At the LP, the mean southward volume transport is −0.4 ± 1.1 Sv, comparable to the −0.8 ± 1.1 Sv reported by Hernández-Guerra et al. (2003) and the −0.8 ± 1.5 Sv reported by Fraile-Nuez et al. (2010) based on four and 9 years of current meter data in the LP, respectively.

Volume transport from PIES data at the LP shows southward flow in spring (−1.1 ± 0.8 Sv) and winter (−0.9 ± 1.0 Sv) and northward in summer (0.2 ± 1.0 Sv) and autumn (0.1 ± 1.0 Sv) (Table 3). This pattern agrees with previous studies (Casanova-Masjoan et al., 2020; Hernández-Guerra et al., 2017; Machín et al., 2006; Pérez-Hernández et al., 2023; Vélez-Belchí et al., 2017), though summer transport is usually southward, with exceptions like the summer 2003 estimates of 1.1 ± 0.5 Sv (Hernández-Guerra et al., 2005).

In autumn, the LP exhibits a northward flow of 0.1 ± 1.0, a feature consistently observed in the region. Stronger mass transport has been reported in previous studies, including 2.9 ± 0.5 Sv in 2014 (Hernández-Guerra et al., 2017), 3.3 ± 0.3 Sv in 2016, and 2.5 ± 0.4 Sv in 2017 (Casanova-Masjoan et al., 2020). However, weaker mass transport was observed, including 1.8 ± 0.1 Sv (Machín et al., 2006), 1.7 ± 0.4 Sv in 2013 (Vélez-Belchí et al., 2017), and 0.5 ± 0.1 Sv (Pérez-Hernández et al., 2013).

The smaller transport estimated by the PIES data in autumn maybe attributed to the seasonal variability of transport in the LP. The GEM method eliminates potential seasonality in volume transport by removing the seasonality variations in temperature and salinity in the shallowest layers (<150 dbar). Similarly, the time series of volume transport from the mooring in the LP as shown in Figure 8b faces a similar limitation, since the shallowest current meter was installed at a depth of 150 m (Fraile-Nuez et al., 2010; Hernández-Guerra et al., 2003).

The northward flow observed at the LP during autumn is attributed to the recirculation of the CC, as evidenced by hydrographic data (Hernández-Guerra et al., 2017), numerical models (Mason et al., 2011), and altimetry data (Pérez-Hernández et al., 2015). Moreover, Pérez-Hernández et al. (2015, 2023) and Vélez-Belchí et al. (2017) proposed that the seasonal behavior of the Atlantic meridional overturning circulation (AMOC) is circulation in

the LP. Although only 1 year of PIES data are available, our findings support the conclusion that the seasonal cycle of the AMOC is linked to the flow along the eastern boundary.

PIES data have proven to be a significant improvement in the quantification of the time-mean and variability of the circulation at the eastern boundary of the North Atlantic subtropical gyre. Maintaining the monitoring system may help assess the interannual variability of the AMOC. To achieve this, the next step involves processing the PIES data collected at the western boundary at 26.5°N as done by Meinen and Garzoli (2014), alongside the PIES data from the eastern boundary.

Conflict of Interest

The authors declare no conflicts of interest relevant to this study.

Data Availability Statement

Pressure Inverted Echo Sounder (PIES) data collected north of the Canary Islands can be found at https://zenodo.org/records/14826982. This study has used other data set publicly available for download in different websites. The hydrographic data were obtained from https://cchdo.ucsd.edu/search?bbox=-20.6443,27.1786,-10.5561,30.7082, and the Argo data were taken from the January 2025 monthly snapshot of the Argo GDAC, in order to include all data available until 31 December 2024 (https://doi.org/10.17882/42182#116315).

Acknowledgments
This study has been performed as part of the Instituto Español de Oceanografía RAPROCAN project and supported by the MAC-CLIMA Project (MAC2/3.5b/254), cofinanced by the INTERREG V-A Spain-Portugal MAC Cooperation Programme (Madeira-Azores-Canary Islands) 2014–2020. This article is a publication of the Unidad Océano y Clima from Universidad de Las Palmas de Gran Canaria, an R&D&I CSIC-associate unit. Verónica Caínzos acknowledges the Agencia Canaria de Investigación, Innovación y Sociedad de la Información (ACIISI) grant program of "Apoyo al personal investigador en formación." We gratefully acknowledge the effort of Adrián Vega Morales, hired by the INVESTIGO program for the employment of young people in research and innovation initiatives under the "Plan de Recuperación, Transformación y Resiliencia," funded by the European Union "NEXT-GENERATION-EU" for processing and plotting PIES data. The authors are grateful to the captain and crew of the R/V Ángeles Alvariño for their help at sea.

References

Barceló-Llull, B., Sangrà, P., Pallàs-Sanz, E., Barton, E. D., Estrada-Allis, S. N., Martínez-Marrero, A., et al. (2017). Anatomy of a subtropical intrathermocline eddy. *Deep-Sea Research Part I*, *124*, 126–139. https://doi.org/10.1016/j.dsr.2017.03.012

Barton, E. D., Aristegui, J., Tett, P., Canton, M., García-Braun, J., Hernández-León, S., et al. (1998). The transition zone of the Canary Current upwelling region. *Progress in Oceanography*, *41*(4), 455–504. https://doi.org/10.1016/S0079-6611(98)00023-8

Book, J. W., Wimbush, M., Imawaki, S., Ichikawa, H., Uchida, H., & Kinoshita, H. (2002). Kuroshio temporal and spatial variations south of Japan determined from inverted echo sounder measurements. *Journal of Geophysical Research*, *107*(C9), 3121. https://doi.org/10.1029/2001JC000795

Borges, R., Hernández-Guerra, A., & Nykjaer, L. (2004). Analysis of sea surface temperature time series of the south-eastern North Atlantic. *International Journal of Remote Sensing*, *25*(5), 869–891. https://doi.org/10.1080/0143116031000082442

Casanova-Masjoan, M., Pérez-Hernández, M. D., Vélez-Belchí, P., Cana, L., & Hernández-Guerra, A. (2020). Variability of the canary current diagnosed by inverse box models. *Journal of Geophysical Research: Oceans*, *125*(8), e2020JC016199. https://doi.org/10.1029/2020JC016199

Chidichimo, M. P., Kanzow, T., Cunningham, S. A., Johns, W. E., & Marotzke, J. (2010). The contribution of eastern-boundary density variations to the Atlantic meridional overturning circulation at 26.5°N. *Ocean Science*, *6*(2), 475–490. https://doi.org/10.5194/os-6-475-2010

Comas-Rodríguez, I., Hernández-Guerra, A., Fraile-Nuez, E., Martínez-Marrero, A., Benítez-Barrios, V. M., Pérez-Hernández, M. D., & Vélez-Belchí, P. (2011). The Azores Current System from a meridional section at 24.5°W. *Journal of Geophysical Research*, *116*(C9), C09021. https://doi.org/10.1029/2011JC007129

Cunningham, S. A., Kanzow, T., Rayner, D., Baringer, M. O., Johns, W. E., Marotzke, J., et al. (2007). Temporal variability of the Atlantic meridional overturning circulation at 26.5°N. *Science*, *317*(5840), 935–938. https://doi.org/10.1126/science.1141304

Donohue, K. A., Watts, D. R., Tracey, K. L., Greene, A. D., & Kennelly, M. (2010). Mapping circulation in the Kuroshio Extension with an array of current and pressure recording inverted echo sounders. *Journal of Atmospheric and Oceanic Technology*, *27*(3), 507–527. https://doi.org/10.1175/2009JTECHO686.1

Duchez, A., Frajka-Williams, E., Castro, N., Hirschi, J., & Coward, A. (2014). Seasonal to interannual variability in density around the Canary Islands and their influence on the Atlantic meridional overturning circulation at 26°N. *Journal of Geophysical Research: Oceans*, *119*(3), 1843–1860. https://doi.org/10.1002/2013JC009416

Fiekas, V., Elken, J., Müller, T. J., Aitsam, A., & Zenk, W. (1992). A view of the Canary Basin thermocline circulation in winter. *Journal of Geophysical Research*, *97*(C8), 12495–12510. https://doi.org/10.1029/92JC01095

Fraile-Nuez, E., Machín, F., Vélez-Belchí, P., López-Laatzen, F., Borges, R., Benítez-Barrios, V., & Hernández-Guerra, A. (2010). Nine years of mass transport data in the eastern boundary of the North Atlantic Subtropical Gyre. *Journal of Geophysical Research*, *115*(C9), C09009. https://doi.org/10.1029/2010JC006161

Harvey, J., & Arhan, M. (1988). The water masses of the central North Atlantic in 1983—84. *Journal of Physical Oceanography*, *18*(12), 1855–1875. https://doi.org/10.1175/1520-0485(1988)018<1855:TWMOTC>2.0.CO;2

Hernandez-Guerra, A., & Nykjaer, L. (1997). Sea surface temperature variability off north-west Africa: 1981–1989. *International Journal of Remote Sensing*, *18*(12), 2539–2558. https://doi.org/10.1080/014311697217468

Hernández-Guerra, A., Arístegui, J., Cantón, M., & Nykjaer, L. (1993). Phytoplankton pigment patterns in the Canary Islands area as determined using coastal zone colour scanner data. *International Journal of Remote Sensing*, *14*(7), 1431–1437. https://doi.org/10.1080/01431169308953977

Hernández-Guerra, A., Espino-Falcón, E., Vélez-Belchí, P., Dolores Pérez-Hernández, M., Martínez-Marrero, A., & Cana, L. (2017). Recirculation of the Canary Current in fall 2014. *Journal of Marine Systems*, *174*, 25–39. https://doi.org/10.1016/j.jmarsys.2017.04.002

Hernández-Guerra, A., Fraile-Nuez, E., Borges, R., López-Laatzen, F., Vélez-Belchí, P., Parrilla, G., & Müller, T. J. (2003). Transport variability in the Lanzarote passage (eastern boundary current of the North Atlantic subtropical Gyre). *Deep-Sea Research I*, *50*(2), 189–200. https://doi.org/10.1016/S0967-0637(02)00163-2

Hernández-Guerra, A., Fraile-Nuez, E., López-Laatzen, F., Martínez, A., Parrilla, G., & Vélez-Belchí, P. (2005). Canary Current and North Equatorial Current from an inverse box model. *Journal of Geophysical Research*, *110*(C12), C12019. https://doi.org/10.1029/2005JC003032

Hernández-Guerra, A., Machín, F., Antoranz, A., Cisneros-Aguirre, J., Gordo, C., Marrero-Díaz, A., et al. (2002). Temporal variability of mass transport in the Canary Current. *Deep Sea Research II*, *49*(17), 3415–3426. https://doi.org/10.1016/S0967-0645(02)00092-9

Kanzow, T., Cunningham, S. A., Johns, W. E., Hirschi, J. J.-M., Marotzke, J., Baringer, M. O., et al. (2010). Seasonal variability of the Atlantic meridional overturning circulation at 26.5°N. *Journal of Climate*, *23*(21), 5678–5698. https://doi.org/10.1175/2010JCLI3389.1

Käse, R. H., & Siedler, G. (1982). Meandering of the subtropical front south-east of the Azores. *Nature*, *300*(5889), 245–246. https://doi.org/10.1038/300245a0

Laiz, I., Pelegrí, J. L., Machín, F., Sangrà, P., Hernández-Guerra, A., Marrero-Díaz, A., & Rodríguez-Santana, A. (2012). Eastern boundary drainage of the North Atlantic subtropical gyre. *Ocean Dynamics*, *62*(9), 1287–1310. https://doi.org/10.1007/s10236-012-0560-6

Machín, F., Hernández-Guerra, A., & Pelegrí, J. L. (2006). Mass fluxes in the Canary Basin. *Progress in Oceanography*, *70*(2–4), 416–447. https://doi.org/10.1016/j.pocean.2006.03.019

Machín, F., Pelegrí, J. L., Fraile-Nuez, E., Vélez-Belchí, P., López-Laatzen, F., & Hernández-Guerra, A. (2010). Seasonal flow reversals of intermediate waters in the canary current system east of the Canary Islands. *Journal of Physical Oceanography*, *40*(8), 1902–1909. https://doi.org/10.1175/2010JPO4320.1

Marcello, J., Hernández-Guerra, A., Eugenio, F., & Fonte, A. (2011). Seasonal and temporal study of the northwest African upwelling system. *International Journal of Remote Sensing*, *32*(7), 1843–1859. https://doi.org/10.1080/01431161003631576

Mason, E., Colas, F., Molemaker, J., Shchepetkin, A. F., Troupin, C., McWilliams, J. C., & Sangrà, P. (2011). Seasonal variability of the Canary Current: A numerical study. *Journal of Geophysical Research*, *116*(C6), C06001. https://doi.org/10.1029/2010JC006665

Meinen, C. S., Piola, A. R., Perez, R. C., & Garzoli, S. L. (2012). Deep Western Boundary Current transport variability in the South Atlantic: Preliminary results from a pilot array at 34.5°S. *Ocean Science*, *8*(6), 1041–1054. https://doi.org/10.5194/os-8-1041-2012

Meinen, C. S. (2001). Structure of the North Atlantic current in stream-coordinates and the circulation in the Newfoundland basin. *Deep-Sea Research I*, *48*(7), 1553–1580. https://doi.org/10.1016/S0967-0637(00)00103-5

Meinen, C. S., & Garzoli, S. L. (2014). Attribution of deep western boundary current variability at 26.5°N. *Deep Sea Research Part I: Oceanographic Research Papers*, *90*(1), 81–90. https://doi.org/10.1016/j.dsr.2014.04.016

Meinen, C. S., Johns, W. E., Garzoli, S. L., van Sebille, E., Rayner, D., Kanzow, T., & Baringer, M. O. (2013). Variability of the deep western boundary current at 26.5°N during 2004–2009. *Deep Sea Research II*, *85*, 154–168. https://doi.org/10.1016/j.dsr2.2012.07.036

Meinen, C. S., & Luther, D. S. (2003). Comparison of methods of estimating mean synoptic current structure in "stream coordinates" reference frames with an example from the Antarctic Circumpolar Current. *Deep-Sea Research I*, *50*(2), 201–220. https://doi.org/10.1016/S0967-0637(02)00168-1

Meinen, C. S., Speich, S., Perez, R. C., Dong, S., Piola, A. R., Garzoli, S. L., et al. (2013). Temporal variability of the meridional overturning circulation at 34.5°S: Results from two pilot boundary arrays in the South Atlantic. *Journal of Geophysical Research: Oceans*, *118*(12), 6461–6478. https://doi.org/10.1002/2013JC009228

Meinen, C. S., Speich, S., Piola, A. R., Ansorge, I., Campos, E., Kersalé, M., et al. (2018). Meridional overturning circulation transport variability at 34.5°S during 2009–2017: Baroclinic and barotropic flows and the dueling influence of the boundaries. *Geophysical Research Letters*, *45*(9), 4180–4188. https://doi.org/10.1029/2018GL077408

Meinen, C. S., & Watts, D. R. (1998). Calibrating inverted echo sounders equipped with pressure Sensors. *Journal of Atmospheric and Oceanic Technology*, *15*(6), 1339–1345. https://doi.org/10.1175/1520-0426(1998)015<1339:CIESEW>2.0.CO;2

Meinen, C. S., & Watts, D. R. (2000). Vertical structure and transport on a transect across the North Atlantic Current near 42°N: Time series and mean. *Journal of Geophysical Research*, *105*(C9), 21869–21891. https://doi.org/10.1029/2000JC900097

Mielke, C., Frajka-Williams, E., & Baehr, J. (2013). Observed and simulated variability of the AMOC at 26°N and 41°N. *Geophysical Research Letters*, *40*(6), 1–6. https://doi.org/10.1002/grl.50233

Mittelstaedt, E. (1983). The upwelling area off Northwest Africa—A description of phenomena related to coastal upwelling. *Progress in Oceanography*, *12*(3), 307–331. https://doi.org/10.1016/0079-6611(83)90012-5

Nykjær, L., & Van Camp, L. (1994). Seasonal and interannual variability of coastal upwelling along northwest Africa and Portugal from 1981 to 1991. *Journal of Geophysical Research*, *99*(C7), 14197–14207. https://doi.org/10.1029/94JC00814

Pacheco, M. M., & Hernandez-Guerra, A. (1999). Seasonal variability of recurrent phytoplankton pigment patterns in the Canary Islands area. *International Journal of Remote Sensing*, *20*(7), 1405–1418. https://doi.org/10.1080/014311699212795

Park, J.-H., Watts, D. R., Tracey, K. L., & Mitchell, D. A. (2005). A multi-index GEM technique and its Application to the Southwestern Japan/East Sea. *Journal of Atmospheric and Oceanic Technology*, *22*(8), 1282–1293. https://doi.org/10.1175/JTECH1778.1

Pérez-Hernández, M. D., Hernández-Guerra, A., Cana-Cascallar, L., Arumí-Planas, C., Caínzos, V., González-Santana, A. J., et al. (2023). The seasonal cycle of the eastern boundary currents of the North Atlantic subtropical Gyre. *Journal of Geophysical Research: Oceans*, *128*(4), e2022JC019487. https://doi.org/10.1029/2022JC019487

Pérez-Hernández, M. D., Hernández-Guerra, A., Fraile-Nuez, E., Comas-Rodríguez, I., Benítez-Barrios, V. M., Domínguez-Yanes, J. F., et al. (2013). The source of the Canary current in fall 2009. *Journal of Geophysical Research: Oceans*, *118*, 1–18. https://doi.org/10.1002/jgrc.20227

Pérez-Hernández, M. D., McCarthy, G. D., Vélez-Belchí, P., Smeed, D. A., Fraile-Nuez, E., & Hernández-Guerra, A. (2015). The canary basin contribution to the seasonal cycle of the Atlantic meridional overturning circulation at 26°N. *Journal of Geophysical Research: Oceans*, *120*(11), 7237–7252. https://doi.org/10.1002/2015JC010969

Rodrigues, R. R., Wimbush, M., Watts, D. R., Rothstein, L. M., & Ollitrault, M. (2010). South Atlantic mass transports obtained from subsurface float and hydrographic data. *Journal of Marine Research*, *68*(6), 819–850. https://doi.org/10.1357/002224010796673858

Sangrà, P., Pascual, A., Rodríguez-Santana, Á., Machín, F., Mason, E., McWilliams, J. C., et al. (2009). The Canary Eddy Corridor: A major pathway for long-lived eddies in the subtropical North Atlantic. *Deep-Sea Research I*, *56*(12), 2100–2114. https://doi.org/10.1016/j.dsr.2009.08.008

Stramma, L. (1984). Geostrophic transport in the Warm Water Sphere of the eastern subtropical North Atlantic. *Journal of Marine Research*, *42*(3), 537–558. https://doi.org/10.1357/002224084788506022

Stramma, L., & Isemer, H.-J. (1988). Seasonal variability of meridional temperature fluxes in the eastern North Atlantic Ocean. *Journal of Marine Research*, *46*(2), 281–299. https://doi.org/10.1357/002224088785113577

Stramma, L., & Siedler, G. (1988). Seasonal changes in the North Atlantic subtropical gyre. *Journal of Geophysical Research*, *93*(C7), 8111–8118. https://doi.org/10.1029/JC093iC07p08111

Sun, C., & Watts, D. R. (2001). A circumpolar gravest empirical mode for the Southern Ocean hydrography. *Journal of Geophysical Research*, *106*(C2), 2833–2855. https://doi.org/10.1029/2000JC900112

Tracey, K. L., & Watts, D. R. (1986). On Gulf Stream meander characteristics near Cape Hatteras. *Journal of Geophysical Research*, *91*(C6), 7587–7602. https://doi.org/10.1029/JC091iC06p07587

Tychensky, A., Le Traon, P.-Y., Hernandez, F., & Jourdan, D. (1998). Large structures and temporal change in the Azores Front during the SEMAPHORE experiment. *Journal of Geophysical Research*, *103*(C11), 25009–25027. https://doi.org/10.1029/98JC00782

Van Camp, L., Nykjaer, L., Mittelstaedt, E., & Schlittenhardt, P. (1991). Upwelling and boundary circulation off Northwest Africa as depicted by infrared and visible satellite observations. *Progress in Oceanography*, *26*(4), 357–402. https://doi.org/10.1016/0079-6611(91)90012-B

Vélez-Belchí, P., Caínzos, V., Romero, E., Casanova-Masjoan, M., Arumí-Planas, C., Santana-Toscano, D., et al. (2021). The Canary intermediate poleward undercurrent: Not another poleward undercurrent in an eastern boundary upwelling system. *Journal of Physical Oceanography*, *51*(9), 2973–2990. https://doi.org/10.1175/JPO-D-20-0130.1

Vélez-Belchí, P., Pérez-Hernández, M. D., Casanova-Masjoan, M., Cana, L., & Hernández-Guerra, A. (2017). On the seasonal variability of the Canary Current and the Atlantic meridional overturning circulation. *Journal of Geophysical Research: Oceans*, *122*(6), 4518–4538. https://doi.org/10.1002/2017JC012774

Watts, D. R., Sun, C., & Rintoul, S. (2001). A two-dimensional gravest empirical mode determined from hydrographic observations in the subantarctic front. *Journal of Physical Oceanography*, *31*(8), 2186–2209. https://doi.org/10.1175/1520-0485(2001)031<2186:ATDGEM>2.0.CO;2

Yang, J. (2015). Local and remote wind stress forcing of the seasonal variability of the Atlantic Meridional Overturning Circulation (AMOC) transport at 26.5°N. *Journal of Geophysical Research: Oceans*, *120*(4), 2488–2503. https://doi.org/10.1002/2014JC010317

Zhao, J., & Johns, W. (2014). Wind-driven seasonal cycle of the Atlantic meridional overturning circulation. *Journal of Physical Oceanography*, *44*(6), 1541–1562. https://doi.org/10.1175/JPO-D-13-0144.1